UNIVERSITY OF BIRMINGHAM

Research at Birmingham

A novel hybrid method combining ASP with PECVD for in-situ low temperature synthesis of vertically aligned carbon nanotube films

Ji, Xiaochao; Li, Xiaoying; Dong, Hanshan

[Link to publication on Research at Birmingham portal](#)

A novel hybrid method combining ASP with PECVD for *in-situ* low temperature synthesis of vertically aligned carbon nanotube films

Xiaochao Ji[a,b], Wei Zhang[b*], Xiaoying Li[a], Helong Yu[b], Hanshan Dong[a*]

[a] *School of Metallurgy and Materials, The University of Birmingham, Birmingham B15 2TT, UK*

[b] *National Key Laboratory for Remanufacturing, AAFE, Beijing 100072, China.*

Abstract: In this study, an in-situ low temperature method to cost-effectively grow vertically aligned carbon nanotube (VACNT) films has been developed by combining advanced active screen plasma (ASP) technique with plasma enhanced chemical vapour deposition (PECVD). A novel active screen consisting of 316 stainless steel cylinder with double top lids was designed for the *in-situ* low-cost high-efficient preparation of catalyst films within a PECVD device, and VACNT films were grown from the catalyst films subsequently at low temperatures (≤ 500ºC). The deposited catalyst films and the VACNT films were characterised by SEM, AFM, XRD, Raman and TEM/EDS. The results show that the catalyst films consist of stainless steel nanoparticles with sizes around 50 nm. The growth of the CNTs is related to the PECVD temperature and the density of the CNTs is determined by the status of the catalyst films. The CNTs are multiwalled with nanoparticles at their tips. The mechanisms behind the *in-situ* low temperature synthesis are discussed based on the plasma physics, growth parameters and physical status of the catalyst films.

1

1. Introduction

In the past decades, carbon nanotubes (CNTs) have received significant attention due to their extraordinary electrical, thermal, and mechanical properties. Various deposition methods have been developed to synthesise high quality CNTs such as arc discharge [1], laser ablation [2] and chemical vapour deposition (CVD) etc.

Among these methods, only CVD is feasible to synthesise vertically aligned CNTs (VACNTs) in controlled manner to achieve assembled VACNTs for functional devices. However, thermal CVD is normally carried out at high temperature which is barrier for academic studies and practical applications of CNTs, the high growth temperature (above 600℃) necessary for the deposition of VACNTs also can cause significant degradation or even damage to some thermal sensitive substrates, such as soda lime glass for field emission displays [3, 4].

In addition, the synthesis of VACNT films is a multi-step process consisting of a catalyst pre-coating step and a CNT growth step. Nano-layers of iron, nickel or cobalt catalyst are pre-coated on the substrate by physical vapour deposition (PVD) via sputtering or evaporation methods [5-7] and then the growth of CNTs is carried out using CVD. The multi-step process carried out in different devices involves the transfer of the PVD deposited catalyst film to the next CVD equipment. This will lead to the oxidation of the coated catalyst films and hence reduction in hydrogen atmosphere is essential for restoring their catalytic function. This will reduce the production efficiency, increase the deposition costs, cause contamination and make it difficult to control the growth processes [8, 9]. Consequently, the complicated multi-

step process and the different devices used are main obstacles for the growth of low-cost high-quality VACNT films. Hence, it is a timely task to develop a new synthesis process to cost-effectively deposit catalyst film and low-temperature grow VACNTs in the same apparatus (hereafter named *in-situ*).

One possible approach for cost-effectively depositing catalyst film for the synthesis of VACNT films is to employ the principle of advanced active screen plasma (ASP) alloying technique [10-12]. Recent study of the mechanism of ASP [13] has revealed that the sputtering of the metal active screen by energetic ions (such as N^+ or Ar^+) led to the deposition of metal nanoparticles. Our recent work [11, 14, 15] has demonstrated that when using a 316 austenitic stainless steel screen, catalyst nanoparticles containing Fe, Ni and Cr can be produced efficiently in a cost-effective manner, which served as the catalyst for the successful synthesis of VACNTs using PECVD. The use of ASP could to some extent reduce the cost for catalyst film preparation but this is not an *in-situ* process.

Some studies have been carried out to obtain CNTs at low temperature and to establish the mechanism involved [4, 16-28]. However, there are still some uncertainties of the products by low temperature synthesis process, such as the transition from CNT to carbon nanofiber (CNF) [16], diameter variation, and so on. The fundamental mechanism of plasma enhanced low temperature growth is also not clear [29]. A common view is that plasma can reduce the growth temperature because of the activated ions generated. After all, sufficient energy is required to grow CNTs, for the decomposition of hydrocarbon gases and the subsequent diffusion and precipitation. Researchers attempted to supply activation energy by adjusting the plasma field under the low temperature growth condition, and several researchers

3

reported some promising results [18-20, 30]. However, high energy ions can restrict the growth of CNTs due to the ion bombardment induced etching effect by plasma.

In some cases, researchers achieved the growth of VACNT films at a relatively low temperature by adding grids [18, 20] connected to an additional electrode. Kojima *et al.* indicated that high energy ions can restrict the growth of CNTs and the grid electrode is helpful to suppress the etching effect of plasma [20], while neutral carbon atoms can pass through and react with the catalysts [30, 31]. No CNTs or only few stubby CNTs can be formed without the use of additional electrode mainly due to the ion bombardment [18].

Based on the above discussion, a novel concept has been proposed by synergising the ASP with the PECVD. The aim of this study was to develop a facile route to pioneer the *in-situ* low temperature growth of VACNT films using an rf PECVD equipped with an ASP setting. The stainless steel active screen can be used to prepare catalyst films, to act as an additional electrode to reduce plasma etching effect and to increase thermal radiations. Therefore, stainless steel catalyst films will be *in-situ* deposited by the ASP setting within the PECVD and VACNT films are subsequently synthesized from the catalyst films below 500℃. Various methods were used to characterise the catalyst films and the CNTs and the low temperature growth mechanism was discussed based on the catalyst status, deposition parameters, and the plasma physics.

2.   Experimental

2.1 ASP setting for catalyst films

The catalyst films were prepared by the ASP setting within a commercial rf PECVD (P500, 13.56MHz, Thin Film Solution Ltd). The schematic of the active screen settings is shown in Figure 1(a). Two active screen lids were installed above the

samples which are connected to the bottom electrode. The upper lid (Catalyst Lid 1) is a pure nickel plate and the lower lid (Catalyst Lid 2) and the cylindrical active screen are made from 316 stainless steel (nominal composition (wt.%) 17.2 Cr, 11.7 Ni, 2.2 Mo, 1.3 Mn, 0.6 Si, 0.06 C, 0.026 P, 0.014 S, balance Fe). The distance between the two lids is 0.5 cm and that between the lower lid and the bottom electrode is 1 cm. The hollow cathode formed between the two lids was used to enhance the plasma density in order to sputter catalyst nanoparticles from the active screen lids. Silicon wafers (100) were used as substrates which were put on the worktable. The catalyst film preparation process was conducted under the conditions shown in Table 1. The temperature was measured by a thermocouple attached to the worktable. After the deposition of the catalyst film, the plasma was turned off and the catalyst films were annealed in the ambient of Ar and H_2 until the temperature reached the setting value. The procedures of the low temperature *in-situ* synthesis of VACNT films are schematically shown in Figure 1(b). All the procedures were carried out within the PECVD.
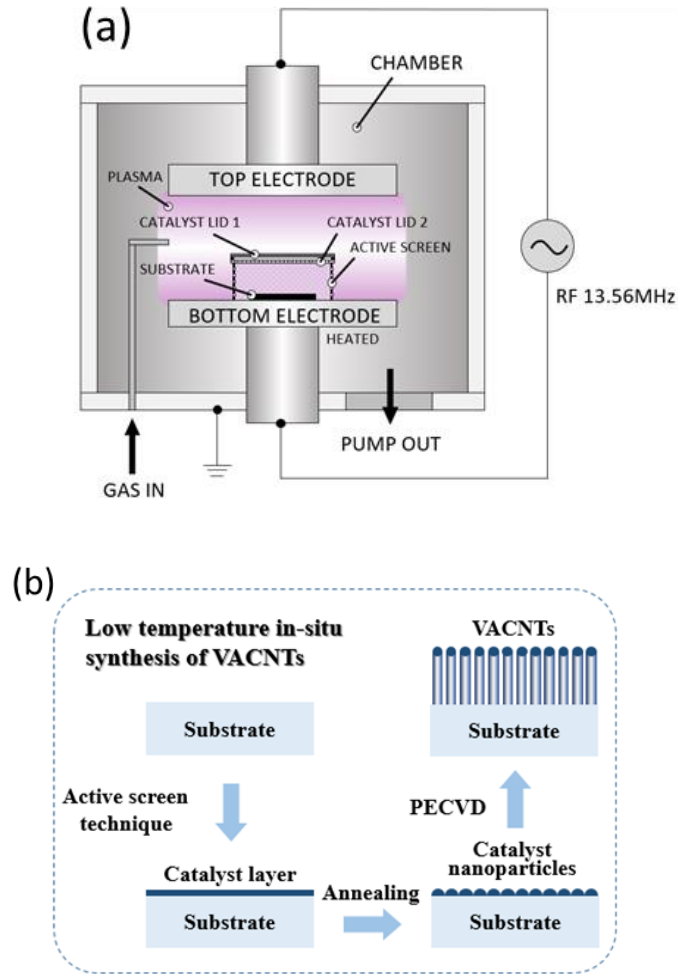
Figure. 1 Schematic diagrams of (a) the PECVD combined with active screen settings and (b) basic procedures of low temperature in-situ synthesis of VACNTs.

Table 1 Preparation conditions for catalyst films by PECVD.

Substrate	Temperature	Time	Power	Pressure	Ar	H_2
Si	300 ℃	10 min	500 W	400 Pa	50 sccm	30 sccm

2.2 VACNTs film growth

After the deposition of catalyst films, the growth of VACNT films was subsequently carried out. The worktable was heated to 300 ℃. Acetylene was introduced as carbon source together with argon and hydrogen. The processes were conducted at 30W for 100 min under different temperatures, working pressures and gas flow rates and the details are summarised in Table 2.

6

Table 2 Growth parameters of VACNT films by PECVD.

Code	Temperature	Time	Pressure	C_2H_2	Ar	H_2
S1	400 ℃	100 min	100 Pa	5 sccm	50 sccm	30 sccm
S2	450 ℃	100 min	100 Pa	5 sccm	50 sccm	30 sccm
S3	500 ℃	100 min	100 Pa	5 sccm	50 sccm	30 sccm
S4	500 ℃	100 min	200 Pa	10 sccm	50 sccm	30 sccm

All substrates are Si coated with catalyst film and the working power is 30 W.

2.3 Characterisation

The surface morphologies of catalyst films and VACNT films were observed by scanning electron microscope (SEM, JEOL 7000). X-Ray Diffraction (XRD) measurement of the catalyst film was detected by a Bruker D8-Advanced diffractometer with Cu Kα radiation (λ=1.54056 Å) including small angle X-ray scattering for thin film analysis. Atomic force microscopy (Nanowizard 3 BioScience AFM) was used to characterise surface morphologies of the catalyst films. The chemical states of the VACNT films were investigated by an X-ray photoemission spectroscopy instrument (XPS, ESCALAB 250Xi), with an Al K_α (1486.8 eV) source, using spot size of 500 μm and binding energy step size of 0.05 eV. Transmission electron microscope (TEM, Oxford JEOL 2100 LaB6) coupled with EDS was employed to analyse nanostructure and composition of the CNTs at an acceleration voltage of 200 kV. TEM specimens were prepared by dispersing CNTs onto a holey carbon film supported by a Cu grid. Raman measurements of the VACNTs were carried out at room temperature using a Renishaw inVia Raman Microscope with a 488 nm excitation and a power of 2mW under ambient condition.

3. Results and discussion

3.1 Microstructure of catalyst films

A series of preliminary screening tests were conducted to identify the optimal

conditions for the deposit of desirable catalyst films with suitable nanoparticles size and good coverage. The experimental results show that the hollow cathode effect (HCE) and hence the sputtering of catalyst nanoparticles can be controlled by the power, the pressure and the distance between two active screen lids. Strong and stable HCE can be achieved under the optimal working conditions shown in Table 1 and the produced plasma (Ar^+ and H^+) density is high sufficient to sputter nanoparticles from the active screen lids to the substrates (Figure 2).

The catalyst film deposited was measured to be about 20nm in thickness and the typical surface morphology is shown in Figure 2(a). Nanoparticles can be clearly observed which are well distributed on the substrate. The size variation of these nanoparticles can lead to the shape and diameter change of the CNTs. However, due to the diffusion and precipitation processes, the extremely large or small sized catalyst nanoparticles may lead to the formation of the carbon onions. Regular and straight CNTs can be formed only from the uniformly sized catalyst nanoparticles [32]. Furthermore, atomic force microscope (AFM) was also utilized to analyse the nanoparticles of the catalyst film (Figure 2(b)). The average roughness of the selected area is 2.6 nm and the deduced site density of the selected area is approximately $10^{11}/cm^2$. Magnified roughness curve of the marked line is also shown in Figure 2(b) and the maximum amplitude is 2.19 nm. Due to the thinness of the film, small angle XRD was employed to analyse the structure of the catalyst film. As shown in Figure 3, three major peaks near 43°, 51° and 75° are corresponding to γ (111), γ (200) and γ (220), which matched the profiles of the austenite stainless steel used for the active screen [15].
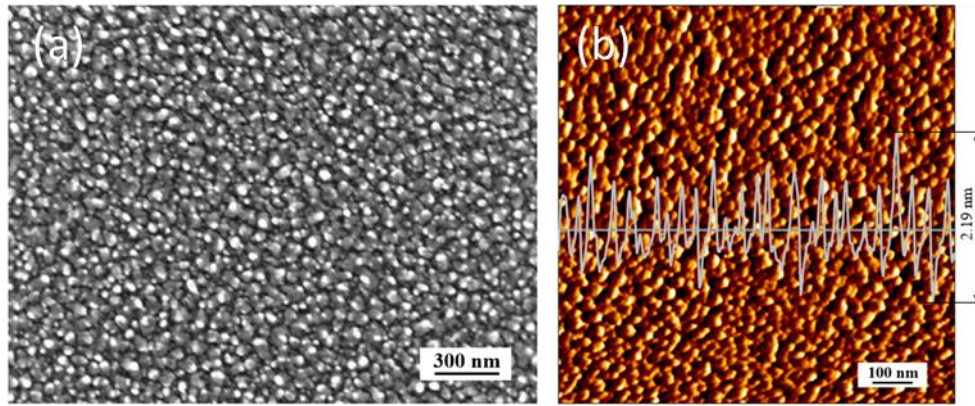
Figure 2 SEM and AFM images of the surface morphology of the in-situ sputtered catalyst film by ASP technique.
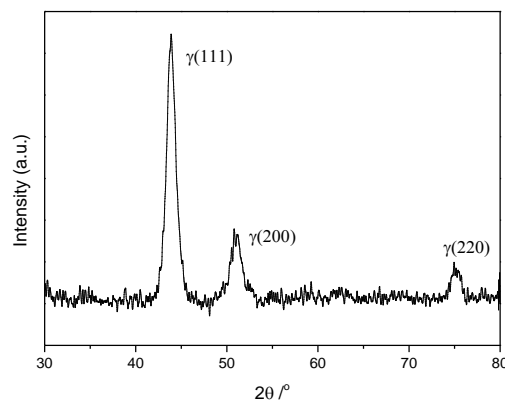
Figure 3 XRD diffraction patterns for catalyst film on Si and typical FeNi γ(111), γ(200) and γ (220) peaks can be identified.

3.2 Microstructure of VACNT films

VACNT films were synthesised from the deposited stainless steel catalyst films at different temperatures. Figure 4 shows the surface morphologies and cross-section views of the VACNT films grown at 400℃, 450℃ and 500℃. The top surfaces of the films show sparsely and curly ends of the CNTs in Figures 4 (a) (c) & (e), while the CNTs are densely packed in the middle and bottom area as a result of the interactions between the neighbour CNTs by Van der Waals forces. Well-aligned structures of the VACNT films were observed from the cross-sections and the results are shown in Figures 4 (b) (d) & (f).

The growth of the CNTs is directly influenced by the catalyst films [33]. **The nucleation efficiency of the catalyst film determines the relationship between**

catalyst nanoparticle density and CNT density [34]. Actually, not all the catalyst nanoparticles are active for the growth of CNTs, while the size and shape of catalyst nanoparticles are changing during the exposure to the gases. The growth of the VACNT films is closely related to the working temperature. The corresponding thickness of the VACNT films formed at 400℃, 450℃ and 500℃ is about 0.9 μm, 1.5 μm and 6 μm. However, no CNTs were formed under the same deposition conditions when the ASP setting was removed. This indicates that the ASP setting has played a key role in the low temperature growth of CNTs.
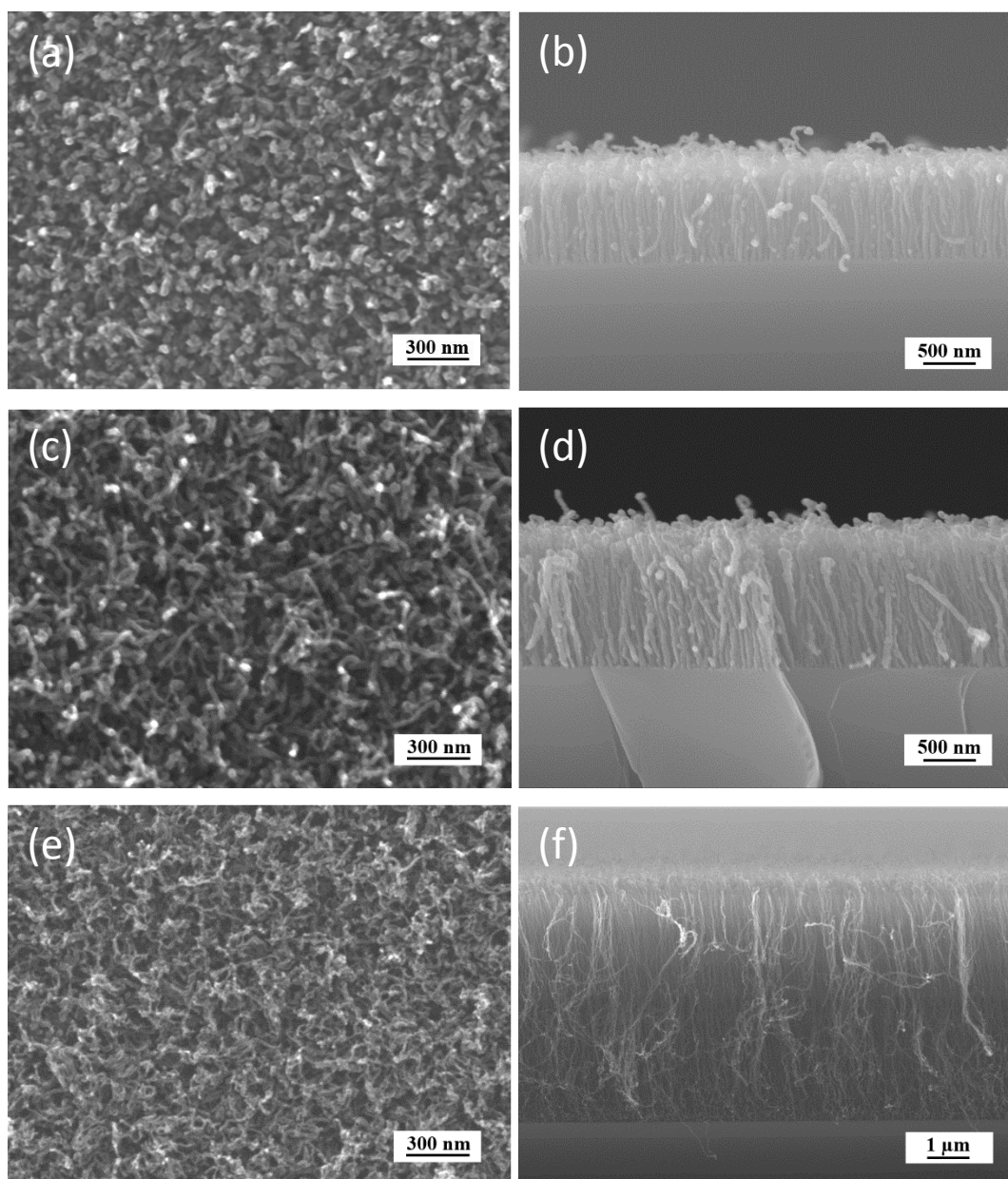
Figure. 4 SEM images of VACNT films deposited at different temperature. (a) & (b) at 400℃; (c) & (d) at 450℃ and (e) & (f) at 500℃.

3.3 Chemical state of VACNTs film

The surface chemical states of the VACNTs film (S2, 450℃) were analysed by X-ray photoelectron spectroscopy (XPS). The spectra shown in Figure 5 were obtained from the top surface before and after etching by argon ions for 50s. Etching by argon was essential for the remove of any contaminates or oxide films from the surface in order to investigate the intrinsic chemical state of the CNTs. Figure 5(a) is the survey spectra and the differences between them were caused by the etching process.

The overlapped low resolution spectra were resolved to analyse the components of C, Fe and Ni. The C-C peak at 284.6 eV appeared in the both spectra. However, a shoulder peak at 286.2 eV corresponding to C-O is more clearly detected from the as-deposited surface, which indicates that carbon in the surface interacted with oxygen when exposed in air after deposition.

Almost no peaks of Fe or Ni were detected from the surface without etching, but obvious Fe $2p_{1/2}$, Fe $2p_{3/2}$ peaks and a weak Ni 2p peak were detected after etching, as shown in Figures 5 (c) & (d). The etching process was effective to remove the carbon coated on the catalyst nanoparticles. The existence of Fe and Ni spectra indicates that the catalysts were still stainless steel nanoparticles, which is consistence with the XRD result.
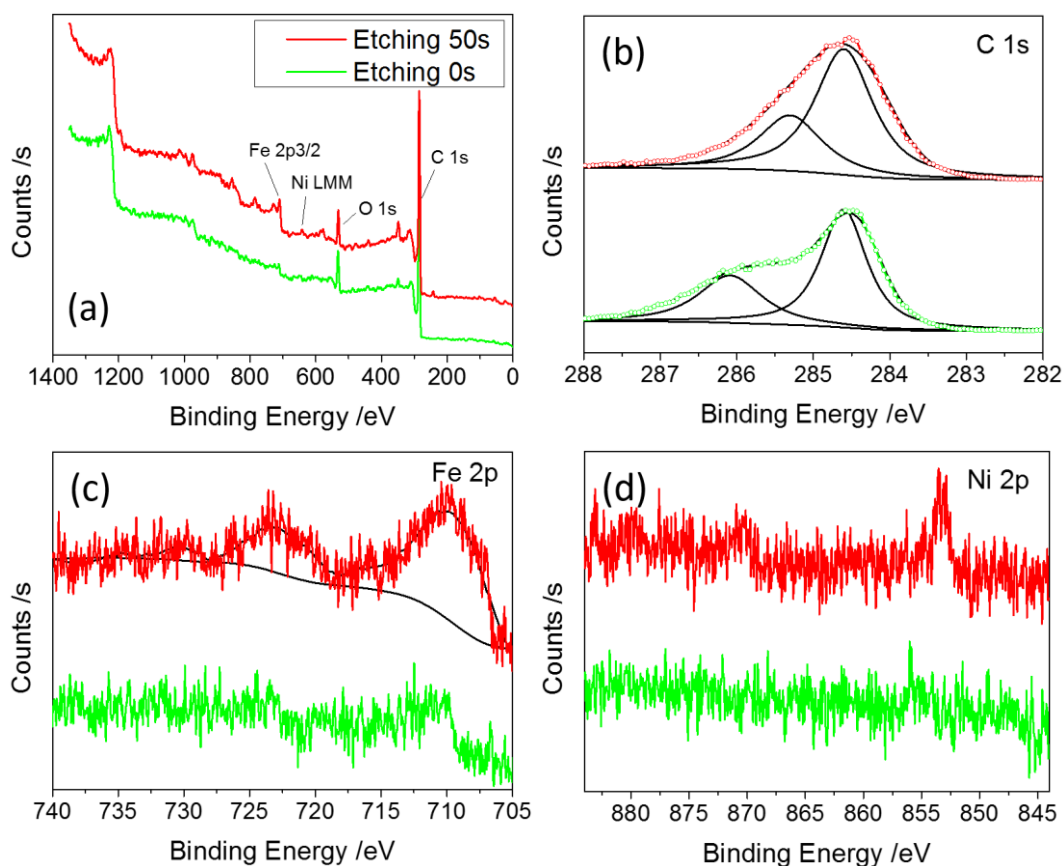
Figure 5 (a) XPS survey spectra of VACNTs film deposited at 450℃ after etching for 0 s and 50 s; (b) high resolution C 1s spectra; (c) high resolution Fe 2p spectra; (d) high resolution Ni 2p spectra.

3.4 TEM results

CNTs were scratched off from the films and the structural details of the CNTs were further studied by TEM. Figures 6 (a), (b) & (c) show the TEM images of the CNTs grown at 400℃, 450℃ and 500℃, respectively. Tubule structures with black dots embedded in the tips of the CNTs can be observed. Judging by the contrast and the EDX results given Figure 7, these black dots are considered as the catalyst nanoparticles deposited by ASP in the catalyst preparation stage. The catalyst nanoparticles were embedded at the tips of the CNTs, and their size and shape have significant influence on the structure and the diameter of the CNTs. However, it is also noted by comparing the CNTs shown in Figures 6(a), (b) and (c) that the lower the growth temperature, the stubbier the CNTs formed. Clearly, growth temperature

12

has also played an important role in the growth of CNTs.

Close observation also found that all the CNTs are multi-walled. Figure 6(d) shows a high resolution TEM image of a CNT synthesized at 450℃, which clearly presents the wall structure. The interlayer distance (about 0.34 nm) is consistent with that of the graphitic layers. It has been reported that the diameters of CNTs are highly related to the growth temperature, the plasma density and the structure of the catalyst particles [32]. In this study, the effect of growth temperature on the diameter of CNTs was studied by using the same plasma density and catalyst films. Figure 6(e) compares the diameter distribution measured from TEM images of CNTs formed at different temperatures. It can be seen that the mean diameter of the CNTs decreased with increasing the growth temperature and the average diameter for the CNTs formed at 400℃, 450℃ and 500℃ is 28 nm, 23 nm and 16 nm, respectively. Due to the relatively low deposition temperature which was not sufficient to cause catalyst particle coarsening. Hence, the decreasing of the diameters may be a result of the **synergistic effect from temperature and plasma in a reducing gas environment [35, 36]**. **Higher deposition temperature in a reducing gas environment** can offer more kinetic energy for the growth of CNTs and can make the catalyst films more dewetted **[37]**, which will promote the diffusion and precipitation of the carbon atoms, and make the growth of CNTs faster and hence thinner.

13
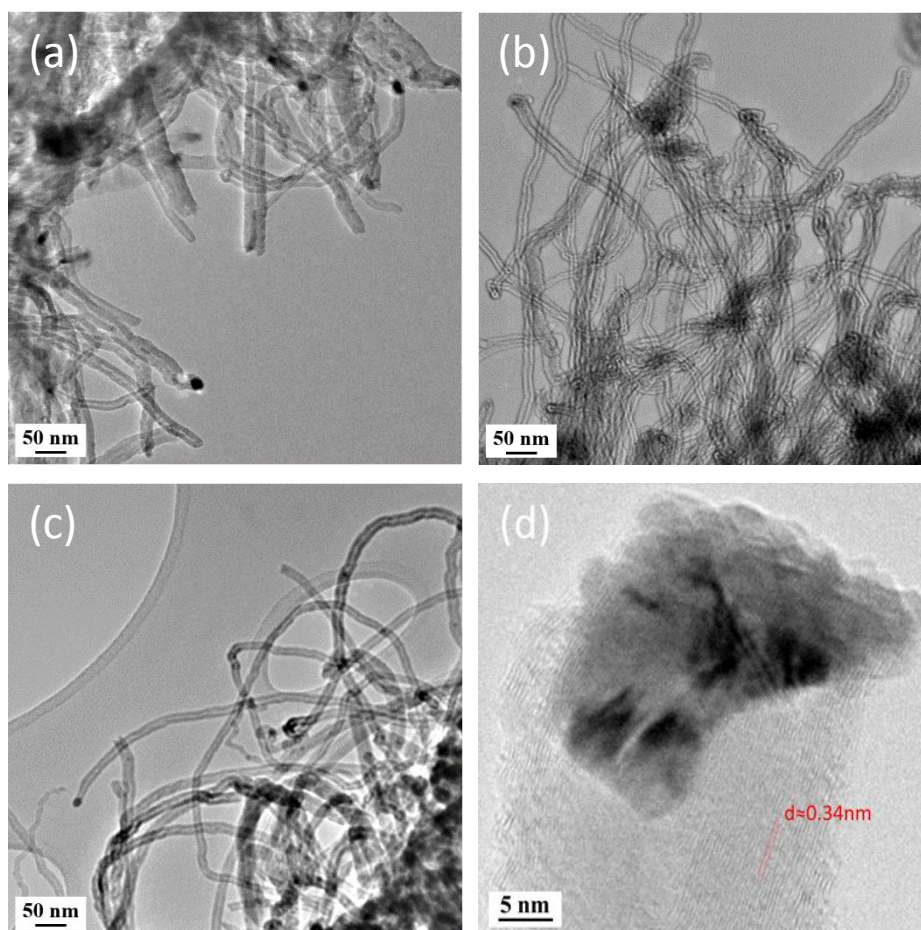
Figure 6 TEM images of CNTs grown at temperature of (a) 400℃, (b) 450℃, (c) 500℃, (d) high resolution image of single carbon nanotube grown at 450℃, and (e) summary of the diameter distribution of CNTs grown at different temperature.

The chemical composition of the deposited CNTs (S2, 450℃) was measured using EDS during TEM analysis and results are shown in Figure 7. As expected, it contained a high amount of carbon content although the experimental error is large for such light element as carbon. A relatively high amount of Cu came from the Cu grid used for TEM. Fe, Ni and Cr were detected and the measured Fe/Ni/Cr weight ratio is

14

6/4.4/1 which is different from that of the 316 SS (3.9/0.7/1). The increased Ni/Fe ratio from 18% for 316 SS to 73% due to the use of a pure Ni lid can improve the efficiency of the catalysts.

Element	Weight %	Atomic %
C	75.32	93.98
Cr	0.6	0.17
Fe	3.62	0.97
Ni	2.62	0.67
Cu	17.84	4.21
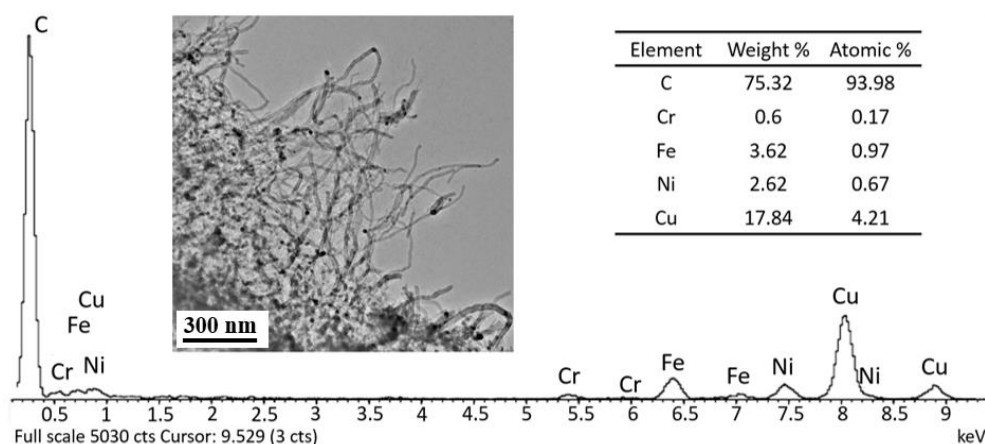
Figure 7 TEM/EDS of the CNTs deposited at 450℃

3.5 Raman results

Raman spectroscopy was used to evaluate the structure and quality of the CNTs produced by the novel in-situ low-temperature plasma process. The Raman spectra of as-deposited VACNT films are shown in Figure 8. Typical D, G, 2D, D+G and 2D' bands can be detected from all these samples, but the peak intensities varied with the synthesis conditions.

D band at around 1350 cm^{-1} is referred as the disorder band which originates from the defects [38]. G band at around 1600 cm^{-1} was caused by the vibration of graphitic carbon atoms. Band at around 2700 cm^{-1} is known as 2D or G' band, which is indicative of the stacked graphene layers and their intensity is correlated to the thickness of the walls. D bands and 2D bands are proportionately increasing with the walls of the nanotubes. The positions and intensities of these bands are affected by the features of the CNTs, such as defects, impurities, wall thickness and element doping [39].

15

In this study, it can be seen from Figure 8 that D band drift to left with the increasing of deposition temperature. The intensity ratios of the D band to the G band (I_D/I_G) for the CNTs formed at different temperatures are around 0.7. When the hydrocarbon gas flow raised from 5sccm to 10sccm (S4), the I_D/I_G ratio increased to 0.97 and the intensity of 2D band became higher.

Intensities of D+G bands and 2D' bands in all spectra are similar. D+G bands have similar information and behaviour to that of the D bands [40]. 2D' bands are too small to evaluate their variations, which have little help in distinguishing the CNTs [40]. No peaks were found in the low frequency areas and the absence of the radial breathing mode (RBM) also verify that the as grown CNTs are MWCNTs. Outer layers of MWCNTs can restrict the breathing mode, which is the primary difference of Raman spectra between SWCNTs and MWCNTs [17].
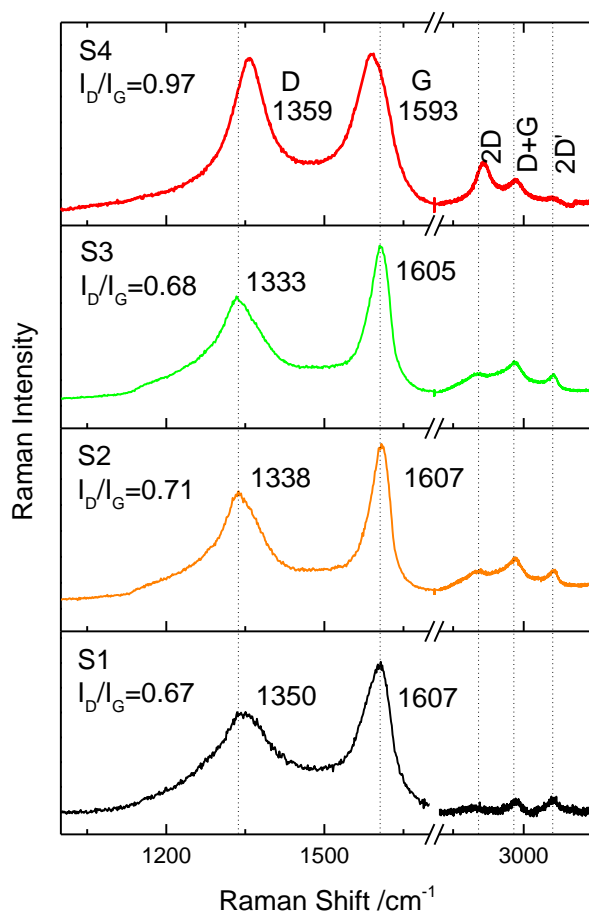
Figure 8 Raman spectra of the VACNT films synthesised at different conditions.

4. Discussion

As reported above, the combination of ASP technique with PECVD has provided a novel approach for *in-situ cost-effective* low temperature synthesis of VACNT films.

4.1 Reduced CVD temperature

The growth of CNTs in this study is believed to be still based on the vapour-liquid-solid mechanism [41]. CNTs formed principally by continuous precipitation of supersaturated carbon atoms which are released from decomposed hydrocarbons and then diffuse into the surface of the catalytic metal particle. The driven force for the diffusion of carbon atoms is ascribed to a temperature gradient. Therefore, sufficient

17

energy is required for the continuous diffusion of carbon atoms. Typical growth temperature for thermal CVD (T-CVD) is above 600℃, and thermal energy is the single source for the decomposition and diffusion processes [42].

In this study, CNTs were successful synthesised at temperatures between 400 and 500 ℃. This could be mainly attributed to the plasma effect brought from PECVD and ASP. First, plasma is effective to ionize the gases which can promote the dissociation of hydrocarbons by increasing the density of ions. Second, plasma has heating effect which can provide more kinetic energy for the diffusion of carbon atoms [21, 43]. Therefore, the growth temperature in PECVD can be much lower than in T-CVD [21, 44].

However, plasma also has an etching effect which can restrict the growth of CNTs. The active screen installed in the PECVD facility between the two electrodes and connected to the bottom electrode has acted as a shield grid to filter or slow down the high-energy ions. This can lead to a desirably balanced function of the plasma, which is necessary for activating the growth process but without causing undue ion etching. In addition, the thermal radiation from the active screen has contributed to the homogenous heating of the substrate surface [45].

4.2 Cost-effective in-situ preparation of catalyst film

As reported, the key to the successful cost-effective in-situ synthesis of VACNT films is to innovatively introduce the principle of ASP into PECVD and the novel design of ASP double lids to enhance the deposition of catalyst film using the hollow-cathode effect.

Basic knowledge of the glow discharge between two plain electrodes is helpful to understand the *in-situ* low temperature growth process of CNTs. Physical appearance of a glow discharge can be mainly divided into cathode dark space, negative glow,

Faraday dark space and positive column [46]. Paschen's Law (Equation 1) presents a relationship for the glow discharge between the breakdown voltage, the pressure and the electrode separation distance [47]. The *in-situ* preparation of the catalyst films was realized by the hollow cathode effect between the two catalyst lids used for the ASP screen, which were controlled by power, pressure, and the distance between two lids. Paschen's Law below provides a basic route to achieve the hollow cathode effect with high density of plasma, which is sufficient to sputter nanoparticles from the lids.

$$V_b = \frac{Bpd}{ln(Apd/ln[1+(1/\gamma)])} \qquad (1)$$

where V_b is the breakdown voltage, p is the pressure inside the chamber, d is the distance between two electrodes, A, B, and γ are constants.

The growth of CNTs are carried out in the dark space where contains a strong electric field [46]. Ions are accelerated to bombard the cathode and secondary electrons are emitted, which accelerate through this space away from the cathode. The settings of the electrodes have a critical effect on the distribution of the plasma field. In this study, the active screen can be counted as an additional electrode, which can expand the cathode dark space to support the growth of CNTs. Besides, the lids also can retain heats by limiting the direct thermal transition from the sample surface to the gas flow, and their thermal radiation effects can promote the low temperature growth of CNTs.

Fe, Co and Ni are common elements used for the growth of CNTs due to their high activity. However, some researchers indicated that some binary or multimetal alloy catalysts are more efficient for the growth of CNTs by increasing the rate of diffusion and reaction [48]. Novel carbon materials like nanocoils or branched CNTs can be deposited from modified composite catalysts [49, 50]. The deposition method in this study has provided a cost-effective way to adjust the composition of the catalysts by

changing the catalyst lids.

In this study, TEM examination has revealed tip growth mode of CNTs, which may be related to the separation of catalyst nanoparticles. It is known that base growth mode happens when there is a strong adhesion between the catalyst particles and the substrates. In some cases, metallic silicide can be generated between the catalysts and the Si substrate [51, 52], which can increase the adhesion. However, these interactions will cause deterioration of the catalysts and typical solution is to add buffer layers, such as SiO_2, Ti, Al [53]. Gohier et al. [54] have indicated that the growth modes are determined by the size of the catalyst particles, which is related to the thickness of the catalyst film and they can cause a transition from the base growth few-wall CNTs to the tip growth multi-wall CNTs [33]. For the tip growth mode, catalyst particle was pulled out from the catalyst film by the growth force of CNTs [55]. However, the pull out process cannot happen when the catalyst particles are too large, thus resulting in a base growth mode [56]. Song et al. [24] reported that the CNT growth mode is not determined by the growth method, even though most PECVD synthesis presented tip growth mode. This is because the strong bombardment effect of the plasma could generate the isolated catalyst particles, which are suitable for the tip growth mode. After all, the growth modes are not only influenced by condition of the catalyst nanoparticles, but also impacted by synthesis parameters such as pressure, temperature, power, etc.

5. Conclusions

In this study, *in-situ* cost-effective low temperature synthesis of VACNT films has been successfully achieved by innovatively introducing the principle of active-screen plasma (ASP) into rf PECVD and the design of novel active screen with double

20

catalyst lids. Fe-Ni-Cr catalyst thin films were *in-situ* prepared by enhanced sputtering based on hollow-cathode effect from both 316 austenitic stainless steel and pure Ni active screen lids, and VACNT films were synthesised subsequently at relatively low temperatures (≤500℃). The active screen set in the PECVD apparatus can be used for high-efficient low-cost catalysts deposition. More importantly, the active screen can also play a key role in the low temperature synthesis of VACNT films by reducing or avoiding undesirable plasma etching effect and providing additional thermal radiation effect. The facile route for the economical and efficient *in-situ* low temperature synthesis of VACNT films developed from this study makes it feasible to cost-effectively fabricate VACNT films on other thermal sensitive materials.

Acknowledgement

References

1.   Iijima, S., *Helical Microtubules of Graphitic Carbon.* Nature, 1991. **354**(6348): p. 56-58.

2.   Thess, A., R. Lee, P. Nikolaev, H.J. Dai, P. Petit, J. Robert, C.H. Xu, Y.H. Lee, S.G. Kim, A.G. Rinzler, D.T. Colbert, G.E. Scuseria, D. Tomanek, J.E. Fischer, and R.E. Smalley, *Crystalline ropes of metallic carbon nanotubes.* Science, 1996. **273**(5274): p. 483-487.

3.   Choi, Y.C., D.J. Bae, Y.H. Lee, B.S. Lee, G.S. Park, W.B. Choi, N.S. Lee, and J.M. Kim, *Growth of carbon nanotubes by microwave plasma-enhanced chemical vapor deposition at low temperature.* Journal of Vacuum Science & Technology A, 2000. **18**(4): p. 1864-1868.

4.   Pitkanen, O., N. Halonen, A.R. Leino, J. Maklin, A. Dombovari, J.H. Lin, G. Toth, and K. Kordas, *Low-Temperature Growth of Carbon Nanotubes on Bi- and Tri-metallic Catalyst Templates.* Topics in Catalysis, 2013. **56**(9-10): p. 522-526.

5.   Bulusheva, L.G., A. Okotrub, A.G. Kudashov, Y.V. Shubin, E. Shlyakhova, N.F. Yudanov, E.M. Pazhetnov, A.I. Boronin, and D.V. Vyalikh, *Effect of Fe/Ni catalyst composition on nitrogen doping and field emission properties of carbon nanotubes.* Carbon, 2008. **46**(6): p. 864-869.

6.   Esconjauregui, S., S. Bhardwaj, J. Yang, C. Castellarin-Cudia, R. Xie, L. D'Arsie, T. Makaryan, H. Sugime, S. Eslava, C. Cepek, and J. Robertson, *Carbon nanotube growth on conductors: Influence of the support structure and catalyst thickness.* Carbon, 2014. **73**: p. 13-24.

7.   Landois, P., A. Peigney, C. Laurent, L. Frin, L. Datas, and E. Flahaut, *CCVD synthesis of carbon nanotubes with W/Co-MgO catalysts.* Carbon, 2009. **47**(3): p. 789-794.

8.   Huang, S.M., Q.R. Cai, J.Y. Chen, Y. Qian, and L.J. Zhang, *Metal-Catalyst-Free Growth of Single-Walled Carbon Nanotubes on Substrates.* Journal of the American Chemical Society, 2009. **131**(6): p. 2094-+.

9.   Li, J.C., P.X. Hou, L.L. Zhang, C. Liu, and H.M. Cheng, *Growth of metal-catalyst-free nitrogen-doped metallic single-wall carbon nanotubes.* Nanoscale, 2014. **6**(20): p. 12065-12070.

10.   Dong, Y.C., X.Y. Li, R. Sammons, and H.S. Dong, *The Generation of Wear-Resistant Antimicrobial Stainless Steel Surfaces by Active Screen Plasma Alloying with N and Nanocrystalline Ag.* Journal of Biomedical Materials Research Part B-Applied Biomaterials, 2010. **93b**(1): p. 185-193.

11.   Dong, Y., X. Li, T. Bell, R. Sammons, and H. Dong, *Surface microstructure and antibacterial property of an active-screen plasma alloyed austenitic stainless steel surface with Cu and N.* Biomedical Materials, 2010. **5**(5).

12.   Chen, J., X.R. Shi, S.J. Qi, M. Mohai, I. Bertoti, Y. Gao, and H.S. Dong, *Reducing and multiple-element doping of graphene oxide using active screen plasma treatments.* Carbon, 2015. **95**: p. 338-346.

13.   Zhao, C., C.X. Li, H. Dong, and T. Bell, *Study on the active screen plasma nitriding and its nitriding mechanism.* Surface & Coatings Technology, 2006. **201**(6): p. 2320-2325.

14.   Dong, Y., X. Li, L. Tian, T. Bell, R.L. Sammons, and H. Dong, *Towards long-lasting antibacterial stainless steel surfaces by combining double glow plasma silvering with active screen plasma nitriding.* Acta Biomaterialia, 2011. **7**(1): p. 447-457.

15.   Lin, K.J., X.Y. Li, L.H. Tian, and H.S. Dong, *Active screen plasma surface co-alloying of 316 austenitic stainless steel with both nitrogen and niobium for the application of bipolar plates in proton exchange membrane fuel cells.* International Journal of Hydrogen Energy, 2015. **40**(32): p. 10281-10292.

16.   Boskovic, B.O., V. Stolojan, R.U.A. Khan, S. Haq, and S.R.P. Silva, *Large-area synthesis of carbon nanofibres at room temperature.* Nature Materials, 2002. **1**(3): p. 165-168.

17. Baro, M., D. Gogoi, A.R. Pal, N.C. Adhikary, H. Bailung, and J. Chutia, *Pulsed PECVD for Low-temperature Growth of Vertically Aligned Carbon Nanotubes.* Chemical Vapor Deposition, 2014. **20**(4-6): p. 161-169.

18. Jang, I., H.S. Uh, H.J. Cho, W. Lee, J.P. Hong, and N. Lee, *Characteristics of carbon nanotubes grown by mesh-inserted plasma-enhanced chemical vapor deposition.* Carbon, 2007. **45**(15): p. 3015-3021.

19. Kang, H.S., H.J. Yoon, C.O. Kim, J.P. Hong, I.T. Han, S.N. Cha, B.K. Song, J.E. Jung, N.S. Lee, and J.M. Kim, *Low temperature growth of multi-wall carbon nanotubes assisted by mesh potential using a modified plasma enhanced chemical vapor deposition system.* Chemical Physics Letters, 2001. **349**(3-4): p. 196-200.

20. Kojima, Y., S. Kishimoto, and T. Mizutani, *Low-temperature growth of carbon nanotubes by grid-inserted plasma-enhanced chemical vapor deposition.* Japanese Journal of Applied Physics Part 1-Regular Papers Brief Communications & Review Papers, 2007. **46**(12): p. 8000-8002.

21. Hofmann, S., C. Ducati, J. Robertson, and B. Kleinsorge, *Low-temperature growth of carbon nanotubes by plasma-enhanced chemical vapor deposition.* Applied Physics Letters, 2003. **83**(1): p. 135-137.

22. Hofmann, S., B. Kleinsorge, C. Ducati, A.C. Ferrari, and J. Robertson, *Low-temperature plasma enhanced chemical vapour deposition of carbon nanotubes.* Diamond and Related Materials, 2004. **13**(4-8): p. 1171-1176.

23. Shiratori, Y., H. Hiraoka, and M. Yamamoto, *Vertically aligned carbon nanotubes produced by radio-frequency plasma-enhanced chemical vapor deposition at low temperature and their growth mechanism.* Materials Chemistry and Physics, 2004. **87**(1): p. 31-38.

24. Song, I.K., Y.S. Cho, G.S. Choi, J.B. Park, and D.J. Kim, *The growth mode change in carbon nanotube synthesis in plasma-enhanced chemical vapor deposition.* Diamond and Related Materials, 2004. **13**(4-8): p. 1210-1213.

25. Baro, M. and A. Pal, *Pulsed Plasma Assisted Growth of Vertically Aligned Carbon Nanotubes at Low Temperature on Mo Substrate.* Plasma Chemistry and Plasma Processing, 2015. **35**(1): p. 247-257.

26. Gangele, A., C.S. Sharma, and A.K. Pandey, *Synthesis of Patterned Vertically Aligned Carbon Nanotubes by PECVD Using Different Growth Techniques: A Review.* Journal of Nanoscience and Nanotechnology, 2017. **17**(4): p. 1 - 18.

27. Nessim, G.D., M. Seita, K.P. O'Brien, A.J. Hart, R.K. Bonaparte, R.R. Mitchell, and C.V. Thompson, *Low Temperature Synthesis of Vertically Aligned Carbon Nanotubes with Electrical Contact to Metallic Substrates Enabled by Thermal Decomposition of the Carbon Feedstock.* Nano Letters, 2009. **9**(10): p. 3398-3405.

28. Sugime, H., S. Esconjauregui, L. D'Arsie, J.W. Yang, A.W. Robertson, R.A. Oliver, S. Bhardwaj, C. Cepek, and J. Robertson, *Low-Temperature Growth of Carbon Nanotube Forests Consisting of Tubes with Narrow Inner Spacing Using Co/Al/Mo Catalyst on Conductive Supports.* Acs Applied Materials & Interfaces, 2015. **7**(30): p. 16819-16827.

29. Hofmann, S., G. Csanyi, A.C. Ferrari, M.C. Payne, and J. Robertson, *Surface diffusion: The low activation energy path for nanotube growth.* Physical Review Letters, 2005. **95**(3).

30. Show, Y., *Selective growth of carbon nanotube at low temperate using triode type plasma enhanced CVD method.* Diamond and Related Materials, 2011. **20**(7): p. 1081-1084.

31. Show, Y. and N. Fukuzumi, *Selective growth of CNT by using triode-type radio frequency plasma chemical vapor deposition method.* Diamond and Related Materials, 2007. **16**(4-7): p. 1106-1109.

32. Choi, Y.C., Y.M. Shin, Y.H. Lee, B.S. Lee, G.S. Park, W.B. Choi, N.S. Lee, and J.M. Kim, *Controlling the diameter, growth rate, and density of vertically aligned carbon nanotubes synthesized by microwave plasma-enhanced chemical vapor deposition.* Applied Physics Letters, 2000. **76**(17): p. 2367-2369.

33. Hofmann, S., M. Cantoro, B. Kleinsorge, C. Casiraghi, A. Parvez, J. Robertson, and C. Ducati, *Effects of catalyst film thickness on plasma-enhanced carbon nanotube growth.* Journal of Applied Physics, 2005. **98**(3).

34. Bedewy , M., B. Viswanath, E.R. Meshot, D.N. Zakharov, S.E. A., and A.J. Hart, *Measurement of the dewetting, nucleation, and deactivation kinetics of carbon nanotube population growth by environmental transmission electron microscopy.* Chemistry of Materials, 2016. **28**(11): p. 3804-3813.

35. Pisana, S., M. Cantoro, A. Parvez, S. Hofmann, A. Ferrari, and J. Robertson, *The role of precursor gases on the surface restructuring of catalyst films during carbon nanotube growth.* Physica E: Low-Dimensional Systems and Nanostructures, 2007. **37**(1-2): p. 1-5.

36. Nessim, G., A. Hart, J. Kim, D. Acquaviva, J. Oh, C. Morgan, M. Seita, J. Leib, and C. Thompson, *Tuning of vertically aligned carbon nanotube diameter and areal density through catalyst pre-treatment.* Nano Letters, 2008. **8**(11): p. 3587-3593.

37. Shi, W., J. Li, E.S. Polsen, C.R. Oliver, Y. Zhao, E.R. Meshot, M. Barclay, D.H. Fairbrother, A.J. Hart, and D.L. Plata, *Oxygen-promoted catalyst sintering influences number density, alignment, and wall number of vertically aligned carbon nanotubes.* Nanoscale, 2017. **9**(16): p. 5222-5233.

38. DiLeo, R.A., B.J. Landi, and R.P. Raffaelle, *Purity assessment of multiwalled carbon nanotubes by Raman spectroscopy.* Journal of Applied Physics, 2007. **101**(6).

39. Rajesh, J.A. and A. Pandurangan, *Lanthanum nickel alloy catalyzed growth of nitrogen-doped carbon nanotubes by chemical vapor deposition.* Rsc Advances, 2014. **4**(39): p. 20554-20566.

40. Antunes, E.F., A.O. Lobo, E.J. Corat, V.J. Trava-Airoldi, A.A. Martin, and C. Verissimo, *Comparative study of first- and second-order Raman spectra of MWCNT at visible and infrared laser excitation.* Carbon, 2006. **44**(11): p. 2202-2211.

41. Tessonnier, J.P. and D.S. Su, *Recent Progress on the Growth Mechanism of Carbon Nanotubes: A Review.* Chemsuschem, 2011. **4**(7): p. 824-847.

42. Lopez, D., I.Y. Abe, and I. Pereyra, *Temperature effect on the synthesis of carbon nanotubes and core-shell Ni nanoparticle by thermal CVD.* Diamond and Related Materials, 2015. **52**: p. 59-65.

43. Teo, K.B.K., D.B. Hash, R.G. Lacerda, N.L. Rupesinghe, M.S. Bell, S.H. Dalal, D. Bose, T.R. Govindan, B.A. Cruden, M. Chhowalla, G.A.J. Amaratunga, J.M. Meyyappan, and W.I. Milne, *The significance of plasma heating in carbon nanotube and nanofiber growth.* Nano Letters, 2004. **4**(5): p. 921-926.

44. Wang, H.Y. and J.J. Moore, *Low temperature growth mechanisms of vertically aligned carbon nanofibers and nanotubes by radio frequency-plasma enhanced chemical vapor deposition.* Carbon, 2012. **50**(3): p. 1235-1242.

45. Li, C.X., J. Georges, and X.Y. Li, *Active screen plasma nitriding of austenitic stainless steel.* Surface Engineering, 2002. **18**(6): p. 453-458.

46. Melechko, A.V., V.I. Merkulov, T.E. McKnight, M.A. Guillorn, K.L. Klein, D.H. Lowndes, and M.L. Simpson, *Vertically aligned carbon nanofibers and related structures: Controlled synthesis and directed assembly.* Journal of Applied Physics, 2005. **97**(4).

47. Roth, J.R., *Industrial plasma engineering.* 1995, Bristol ; Philadelphia: Institute of Physics Pub. v. <1 >.

48. Shen, W., Y. Wang, X. Shi, N. Shah, F. Huggins, S. Bollineni, M. Seehra, and G. Huffman, *Catalytic nonoxidative dehydrogenation of ethane over Fe-Ni and Ni catalysts supported on Mg(Al)O to produce hydrogen and easily purified carbon nanotubes.* Energy & Fuels, 2007. **21**(6): p. 3520-3529.

49. Liao, X.Z., A. Serquis, Q.X. Jia, D.E. Peterson, Y.T. Zhu, and H.F. Xu, *Effect of catalyst composition on carbon nanotube growth.* Applied Physics Letters, 2003. **82**(16): p. 2694-2696.

50.   Fu, X., L.J. Pan, D.W. Li, N. Zhou, and Y.M. Sun, *Controlled synthesis of carbon nanocoils with selective coil diameters and structures by optimizing the thickness of catalyst film.* Carbon, 2015. **93**: p. 361-369.

51.   Jung, Y.J., B.Q. Wei, R. Vajtai, and P.M. Ajayan, *Mechanism of selective growth of carbon nanotubes on SiO2/Si patterns.* Nano Letters, 2003. **3**(4): p. 561-564.

52.   Yang, J.W., S. Esconjauregui, A.W. Robertson, Y.Z. Guo, T. Hallam, H. Sugime, G.F. Zhong, G.S. Duesberg, and J. Robertson, *Growth of high-density carbon nanotube forests on conductive TiSiN supports.* Applied Physics Letters, 2015. **106**(8).

53.   Wu, W.Y., F.Y. Teng, and J.M. Ting, *The effect of an Al underlayer on Fe-Si thin film catalysts for the improved growth of carbon nanotubes.* Carbon, 2011. **49**(13): p. 4589-4594.

54.   Gohier, A., C.P. Ewels, T.M. Minea, and M.A. Djouadi, *Carbon nanotube growth mechanism switches from tip- to base-growth with decreasing catalyst particle size.* Carbon, 2008. **46**(10): p. 1331-1338.

55.   Helveg, S., C. Lopez-Cartes, J. Sehested, P.L. Hansen, B.S. Clausen, J.R. Rostrup-Nielsen, F. Abild-Pedersen, and J.K. Norskov, *Atomic-scale imaging of carbon nanofibre growth.* Nature, 2004. **427**(6973): p. 426-429.

56.   Wei, Y.Y., G. Eres, V.I. Merkulov, and D.H. Lowndes, *Effect of catalyst film thickness on carbon nanotube growth by selective area chemical vapor deposition.* Applied Physics Letters, 2001. **78**(10): p. 1394-1396.